Structural and optical properties of $RbTiOPO_4$:Nb crystals

2007 J. Phys.: Condens. Matter 19 116214

(http://iopscience.iop.org/0953-8984/19/11/116214)

IOP PUBLISHING JOURNAL OF PHYSICS: CONDENSED MATTER

J. Phys.: Condens. Matter **19** (2007) 116214 (15pp) doi:10.1088/0953-8984/19/11/116214

Structural and optical properties of $RbTiOPO_4$:Nb crystals

J J Carvajal[1], P Segonds[2], A Peña[1], J Zaccaro[3], B Boulanger[2], F Díaz[1] and M Aguiló[1,4]

[1] Física i Cristal.lografia de Materials (FiCMA), Universitat Rovira i Virgili, Campus Sescelades, c/Marcel.lí Domingo, s/n, E-43007-Tarragona, Spain
[2] Laboratoire de Spectrométrie Physique, Université Joseph Fourier and Centre National de la Recherche Scientifique BP 87, 38402 St Martin d'Hères Cedex, France
[3] Laboratoire de Cristallographie, Centre National de la Recherche Scientifique, 25 Avenue des Martyrs BP 166, 38042 Grenoble Cedex 09, France

E-mail: magdalena.aguilo@urv.net

Received 2 November 2006, in final form 8 February 2007
Published 5 March 2007
Online at stacks.iop.org/JPhysCM/19/116214

Abstract

When dealing with crystals showing self-frequency conversion properties, $RbTiOPO_4$ doped with Nb^{5+} (RTP:Nb) is a better matrix than RTP for hosting luminescent ions in higher concentration. Therefore, we investigated the structural and the non-linear optical properties of RTP:Nb and RTP crystals for comparison. We used a new crystal growth process for RTP:Nb, which provides isometric inclusion- and crack-free crystals. Structural studies show that Nb^{5+} ions are located in Ti positions only, which is confirmed by optical absorption and polarized Raman scattering studies. Moreover, the transparency domain of RTP:Nb is affected in the UV edge and in the IR region by the presence of Nb^{5+} ions. Finally, we found that the fundamental wavelengths of type II angular non-critical phase-matching for second-harmonic generation along the x and y principal axes are smaller in RTP:Nb than in RTP, approaching those of KTP.

1. Introduction

In the past ten years, the literature has widely reported efficient non-linear crystals of the isostructural titanyl phosphate family $MTiOPO_4$ (where M = Na, K, Rb, Cs, Ag, NH_4, or Tl). The most attractive have been $KTiOPO_4$ (KTP) crystals, which are used in numerous laser devices due to their efficient and thermally stable non-linear optical properties for frequency conversion. For example, KTP is a privileged crystal for the second-harmonic generation (SHG) of the wavelength around 1 μm, emitted by neodymium- and ytterbium-based lasers [1]. KTP is also phase-matched for sum- and difference-frequency generation over wavelengths

[4] Author to whom any correspondence should be addressed.

ranging from the visible to the infrared, and it is used for optical parametric amplification (OPA) and optical parametric oscillation (OPO) generating 1.58 μm for eye-safe applications [2]. However, the occurrence of photochromic damage limits the use of KTP in high-power devices.

$RbTiOPO_4$ (RTP) is another compound of the isostructural titanyl phosphate family $MTiOPO_4$. Although RTP was the first known derivative of KTP [3], it has not been intensively studied because the crystal growth as well as the linear and non-linear properties of this material are very close to those of KTP. However, the photochromic damage threshold of RTP—1.8 times higher than that of KTP [4]—makes it more suitable for high-power applications. RTP is also of prime interest for quasi-phase-matched interactions, since thick samples of periodically poled RTP have been designed [5].

Furthermore, crystals with non-linear optical properties for frequency conversion, and doped with lanthanide (Ln^{3+}) photo-luminescent ions, can show self-frequency conversion properties. In previous studies, we reported that RTP is a good matrix for hosting luminescent Ln^{3+} ions at a higher concentration than that obtained in KTP [6]. When RTP is codoped with Nb^{5+} ions (RTP:Nb) it is even a better matrix for hosting Ln^{3+} ions, as their concentration increases and reaches a value high enough to produce an efficient laser emission [7]. This is attributed to the fact that the incorporation of Nb in these crystals expands the cell parameters of the structure of RTP, favouring the incorporation of a larger ion in the structure, as is the case for Ln^{3+}. Nb^{5+} also acts as a charge compensator when Ln^{3+} ions substitute Ti^{4+} in the structure, which stabilizes the electroneutrality of the crystals, allowing a higher concentration of Ln^{3+} ions to be incorporated in the crystals [8].

In the present work we investigate changes caused by the presence of Nb^{5+} ions in the structure and in the optical properties of RTP. In particular, this paper is devoted to $Rb_{0.955}Ti_{0.955}Nb_{0.045}OPO_4$, labelled from now as RTP:Nb, which is a representative example of these changes. First, we report crystal growth and structure studies of RTP:Nb. Secondly, we present polarized light absorption spectra and Raman spectroscopy studies. Finally, we report non-linear optical properties of RTP:Nb including refractive index measurements as a function of the wavelength, and direct measurements of non-critical phase-matching angles for second-harmonic generation (SHG). All the investigated properties of RTP:Nb are discussed in comparison to RTP and KTP.

2. Crystal growth

Because of its incongruent melting, conventional growth techniques from the melt cannot be used for the growth of RTP:Nb crystals. Instead, they were grown by using the TSSG (top-seeded solution growth) slow-cooling method. We considered the Rb_2O–P_2O_5–TiO_2–Nb_2O_5 self-flux system using a molar% composition of 40.8–27.2–31.0–1.0. By using self-flux growth we take advantage that only constituents of the crystal formula are used and then no other impurities are introduced. Moreover, cracks were avoided by using crystal seeds with the same composition as that of the crystal being grown. However, we previously reported that doping with Nb strongly affects the morphology of RTP crystals: they grow as thin plates along the $\boldsymbol{a}$ axis, reducing significantly the dimensions of the sample along this crystallographic direction [9]. Fortunately, this effect could be compensated by using a seed with an $\boldsymbol{a}$-axis dimension thicker than the two others [10]. Then, grown crystals are more isometric, but their $\boldsymbol{a}$-axis dimension is almost the same as that of the crystal seed. With this method, inclusion- and crack-free RTP:Nb crystals were grown with a 4.5 atom% Nb concentration, and with typical dimensions of 5 mm × 5 mm × 5 mm corresponding to the $\boldsymbol{a} \times \boldsymbol{b} \times \boldsymbol{c}$ axes of the crystallographic frame respectively. One as-grown RTP:Nb crystal is depicted in figure 1(a) and the Miller indices of its natural faces are given in figure 1(b).

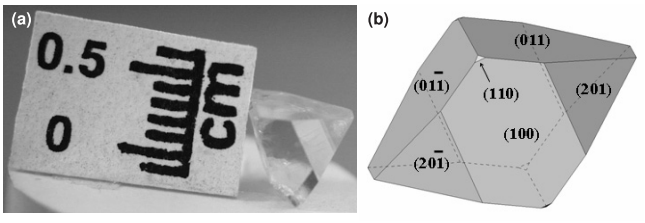

Figure 1. (a) Single crystal of RTP:Nb grown using the acentric crystal growth system described in [9]. It uses crystal seeds of 5.0 mm × 1.5 mm × 3.0 mm in $\boldsymbol{a} \times \boldsymbol{b} \times \boldsymbol{c}$ directions. (b) Miller indices of the natural faces of the RTP:Nb single crystal shown in figure 1(a) on a schematic representation of the theoretical morphology of a RTP:Nb crystal obtained with the shape utility.

The chemical composition of RTP:Nb was determined from the refinement of the structure by single-crystal x-ray diffraction, which is reported in the following section. It corresponds to a stoichiometric formula of $Rb_{0.955}Ti_{0.955}Nb_{0.045}OPO_4$.

3. Structure

We refined the crystal structure of $Rb_{0.955}Ti_{0.955}Nb_{0.045}OPO_4$, labelled as RTP:Nb. These studies were performed at room temperature, by using x-ray diffraction analysis on an as-grown single crystal. The crystal structure was solved by Patterson synthesis and refined by full-matrix least squares using the SHELXS97 utility [11]. We found that RTP:Nb crystallizes in the orthorhombic crystal system with the space group of symmetry $Pna2_1$. The unit cell parameters have the following values: $\boldsymbol{a} = 12.947\ (3)$ Å, $\boldsymbol{b} = 6.498\ (3)$ Å, $\boldsymbol{c} = 10.579\ (7)$ Å, and $Z = 8$. Then, parameter $\boldsymbol{a}$ is smaller, parameter $\boldsymbol{b}$ is slightly larger and parameter $\boldsymbol{c}$ is clearly larger than the corresponding ones in the structure of RTP [12]. This result follows the general trend in the evolution of the cell parameters in RTP when doped with Nb [13].

The structure of the compounds of the titanyl phosphate family $MTiOPO_4$ generally consists of two crystallographically independent TiO_6 octahedra, which are distorted and linked together by sharing corners, forming helical chains oriented along the $\boldsymbol{c}$ axis. These chains are further bridged by PO_4 tetrahedra, in such a way that a three-dimensional network is created. Then, large structural cages are formed in the free spaces left by TiO_6 and PO_4 polyhedra. These spaces are occupied by a monovalent cation (Rb in our case) that is arranged in two non-equivalent crystallographic positions [12].

We also found in RTP:Nb typical long and short Ti–O bonds located in helical chains of TiO_6 octahedra. However, in this crystal the short distances are shorter and the long distances are longer than the corresponding ones in RTP [12]. Then, the distortion of the TiO_6 octahedra in RTP:Nb is larger than that of RTP, which is expected to have implications for the non-linear optical properties [14]. We also found that Nb only substitutes one of the two available Ti crystallographic positions in the unit cell of RTP:Nb structure. In our opinion, this preference has an electrostatic reason rather than a steric one, because the distances between Ti and Rb are shorter for one of the Ti sites compared with the other. This prevents the substitution of Ti^{4+} by a cation with a larger electrical charge, as is the case for Nb^{5+}, and it is self-compensated electrically by the creation of vacancies for monovalent cation Rb. Note that this feature was observed in KTP:Nb [15, 16].

Finally, the structure of RTP:Nb is the enantiomorphic image of RTP. This means that the atomic positions in this structure correspond to those of RTP by the reflection in a mirror plane located at almost a quarter of the cell parameter along the $\boldsymbol{c}$ axis. This observation has

Table 1. UV transmission cut-off wavelengths, $\lambda_{\text{cut-off}}$, in nanometres, given at a 1/e-factor from the maximum value of the transmittance for RTP and RTP:Nb.

Crystal	$E \parallel b$ $\lambda_{\text{cut-off}}$	$E \parallel c$ $\lambda_{\text{cut-off}}$	Maximum value of the transmittance (%)
RTP	338	342	89.0
RTP:Nb	345	350	85.8

also already been reported in the structure of KTP:Nb when compared to that of KTP [15, 16]. Then, we can assert that similar trends occur in the structure of RTP and KTP when doped with Nb^{5+} ions.

4. Transmission spectra

Generally, the transparency domain for KTP isostructurals ranges between 0.35 and 4.5 μm [17], and due to the anisotropic nature of this family of crystals polarized light transmission spectra are recorded [18]. We performed such studies in RTP and RTP:Nb crystals cut as slabs polished to optical quality and with their input and output faces oriented perpendicularly to the $\boldsymbol{a}$ axis. All the RTP and RTP:Nb slabs were 1 mm thick, but we also cut 50 μm thick slabs for studies of the IR band edge. The linear polarization of the incident beam was oriented along the $\boldsymbol{b}$- and $\boldsymbol{c}$ axis successively. The measurements were carried out between 0.1 and 3.0 μm by using a Cary 500 spectrophotometer and between 3.0 and 9.0 μm by using a Midac Prospect Fourier-transform IR (FTIR) spectrometer. A Glan–Thompson quartz polarizer was used in the Cary 500 spectrophotometer to record polarized light spectra. With the Midac Prospect FTIR spectrometer, we studied unpolarized light spectra in N_2 atmosphere, avoiding the adsorption of water vapour from the atmosphere on samples.

With the Cary 500 spectrophotometer, we first recorded absorption spectra of RTP:Nb in the visible, before and after annealing at 773 K during 3 h in air. We observed two broad absorption bands centred at 594 and 639 nm that disappear after annealing, and that may be related to the presence of Ti^{3+} which oxidizes to Ti^{4+} during annealing [19]. This means that the substitution of Ti^{4+} by Nb^{5+} is compensated by two different mechanisms: (i) the creation of Rb vacancies as we have already reported in the previous section and (ii) the presence of Ti^{3+} in the structure.

The ultraviolet (UV) absorption edge in the isostructural titanyl phosphate family $MTiOPO_4$ is generally attributed to the absorption of light by the Ti–O subgroups [17]. We recorded low-resolution transmission spectra in RTP:Nb and in RTP for comparison and took special care to record the polarized light transmission and optical absorption spectra at the UV band edge, to study the effects of substitution of Ti by Nb in their structure. They are shown in figures 2(a) and (b), for RTP:Nb and RTP, respectively, and table 1 gives the UV cut-off wavelengths determined at a 1/e-factor from the maximum value of the transmittance. Our data show that the maximum value of transmittance is 5% higher for RTP than that of RTP:Nb, and it is higher with light linearly polarized parallel to the $\boldsymbol{b}$ axis rather than to the $\boldsymbol{c}$ axis in both crystals. We can also see from figures 2(c) and (d) and table 2 that the value of the cut-off wavelength, $\lambda_{\text{cut-off}}$, is larger in RTP:Nb for both polarization schemes, which is in agreement with the reported values of $\lambda_{\text{cut-off}}$ around 400 nm in $KNbO_3$ [20] and around 350 nm in KTP [17].

With the FTIR spectrometer we studied IR unpolarized transmission spectra from 2.6 to 9.0 μm that are reported in figures 3(a) and (b) for RTP and RTP:Nb respectively. Such spectra generally show a band edge, which is caused by the first and second overtones of the two bond

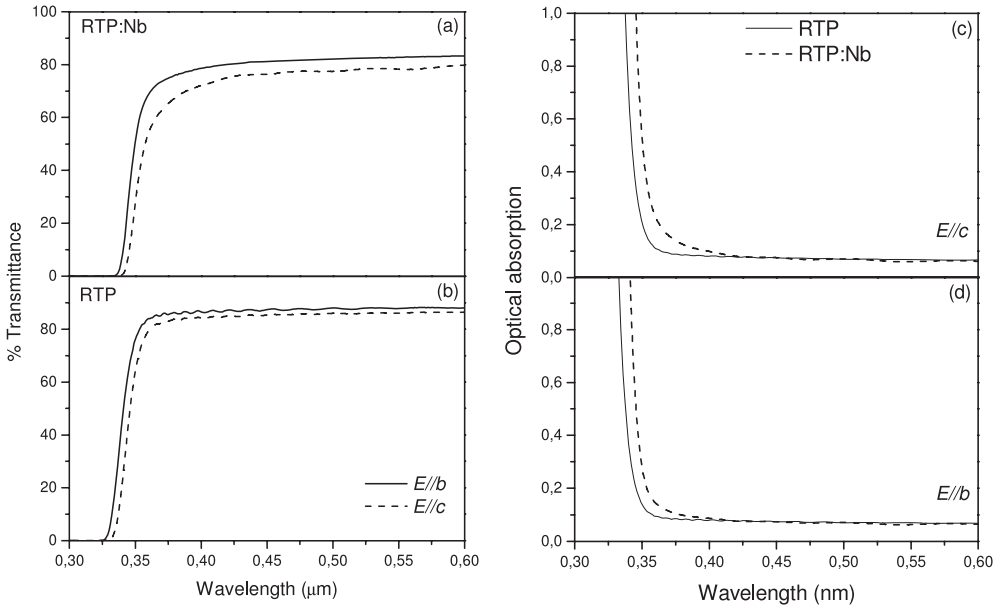

Figure 2. Transmission spectra of RTP:Nb (a) and of RTP (b) measured as a function of the wavelength in the UV region for a propagation along the $\boldsymbol{a}$ axis and for the linear polarization parallel to the $\boldsymbol{b}$ axis (solid line) and to the $\boldsymbol{c}$ axis (dashed line). Optical absorption spectra of RTP (solid line) and of RTP:Nb (dashed line) measured as a function of the wavelength in the UV region for a propagation along the $\boldsymbol{a}$ axis for the linear polarization parallel to the $\boldsymbol{c}$ axis (c) and for the linear polarization parallel to the $\boldsymbol{b}$ axis (d).

Table 2. Position of the absorption bands in the IR region marked out in wavelengths and in wavenumbers and their assignment for RTP:Nb.

Position		
Wavelength (μm)	Wavenumber (cm^{-1})	Assignation
2.8	3475	Tensions of H_2O with H-bonds
3.4	2900	Second overtone ν_3 of PO_4
4.6–5.2	2153–1907	First overtone ν_3 of PO_4
5.4–5.8	1709–1835	First overtone ν_1 of PO_4
5.9–6.9	1463–1690	Combination bands ($\nu_3 + \nu_4$) of PO_4
7.6–8.1	1227–1511	Combination bands ($\nu_1 + \nu_2$) of PO_4

stretching ν_3 and ν_1 vibrations of the PO_4 tetrahedra [17]. The value of this IR absorption edge has been reported to depend on the thickness for KTP crystals [17]. By recording the transmission spectra in two samples of RTP with different thicknesses (1 mm and 50 μm), we corroborated these results as shown in figure 3(a). Comparing the transmission spectra in the IR region between 50 μm thick RTP:Nb and RTP crystals (see figures 3(a) and (b)) we found similar slopes and no shifting of the vibrational bands in this region when Nb is introduced in the RTP crystal. This observation corroborates that Nb only substitutes Ti positions in the RTP:Nb structure, as was expected from the results of x-ray diffraction [8].

Table 2 gives the position of the absorption bands in microns and in cm^{-1}, as well as their assignment for RTP:Nb, between 2 and 8 μm. The internal vibrations of a regular PO_4 tetrahedron have been defined as non-degenerate ν_1, double degenerate ν_2 and triply degenerate

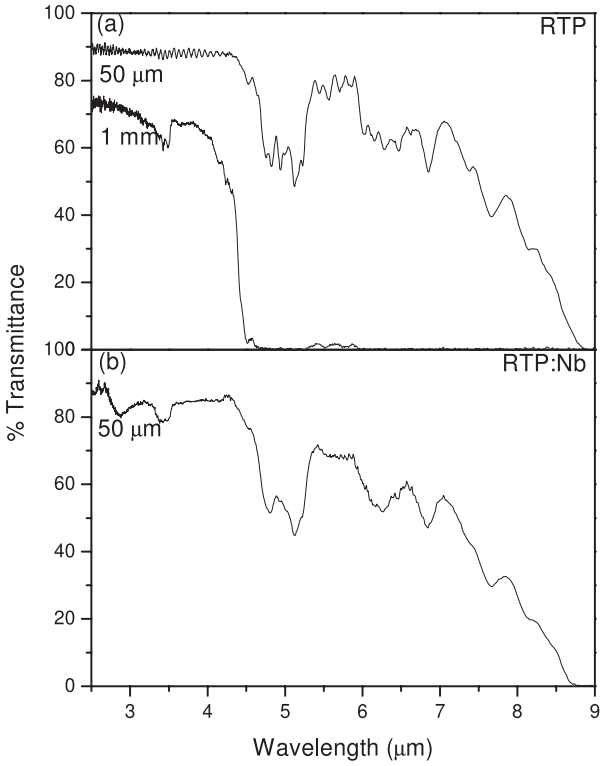

Figure 3. (a) IR unpolarized transmission spectra from 2.6 to 9 μm for RTP as a function of the wavelength for two thicknesses of RTP slabs. (b) IR unpolarized transmission spectra from 2.6 to 9 μm for a 50 μm thick RTP:Nb slab.

ν_3 and ν_4 modes [21]. When the PO_4 tetrahedron is slightly deformed, the degeneracy of the ν_2, ν_3 and ν_4 modes breaks, generating a higher number of bands than in the regular PO_4 tetrahedron [22]. We found that this is the case for RTP and RTP:Nb since the first overtone of the ν_3 consists of six peaks located between 4.6 and 5.2 μm (1907 and 2153 cm^{-1}), as shown in figures 3(a) and (b). Note that their wavelength (wavenumber) is longer (smaller) than the ones in KTP [17]. This is probably due to the difference in the bond distance between P and O when comparing RTP or RTP:Nb to KTP [12]. In the range between 5.4 and 5.8 μm (1709 and 1835 cm^{-1}) a series of bands in RTP and a broad band in RTP:Nb crystals have been observed (see figures 3(a) and (b)) that can be related to the first overtone of the ν_1 vibration of the phosphate group [17]. Furthermore, several bands appear at longer wavelengths for both crystals. They may correspond to a combination of bands derived from the sum or difference of two or more fundamental vibrations of the PO_4 group [17]. For example, the groups of bands ranging between 5.9 and 6.9 μm (1430 and 1690 cm^{-1}) match with the summation of $(\nu_3 + \nu_4)$ vibrations and the groups of bands centred at 7.6 and 8.1 μm (1225 and 1300 cm^{-1}) match with the summation of $(\nu_1 + \nu_2)$ vibrations. Then, the two distorting ν_2 and ν_4 vibrations of the PO_4 tetrahedron, whose fundamental modes are expected to appear between 20 and 25 μm, can interact with the ν_1 and ν_3 vibrations, generating new bands in the IR region where the band edge is observed. Finally, while no bands attributed to OH^- are observed in RTP, one appears at 2.8 μm (3475 cm^{-1}) in RTP:Nb. OH^- bands are generally attributed to the adsorption of

water from the environment by the crystal, which seems to indicate that the RTP:Nb crystals are a little more hygroscopic than pure RTP crystals.

5. Raman analysis

The literature has already reported an extensive polarized Raman scattering study of KTP [23], leading to chemical and structural information of the crystal, including bondings. No such information about RTP:Nb or RTP has been published yet. It is given in this section from a detailed analysis of spontaneous Raman scattering measurements. For this study RTP:Nb and RTP crystals were cut as a slab with dimensions of around 2 mm × 2 mm × 2 mm and with six faces polished and oriented perpendicularly to the three crystallographic axes $\boldsymbol{a}$, $\boldsymbol{b}$ and $\boldsymbol{c}$. Since RTP and RTP:Nb structures crystallize in the orthorhombic system, the $\boldsymbol{a}$-, $\boldsymbol{b}$- and $\boldsymbol{c}$-axes correspond to the x-, y- and z-axes of the dielectric frame respectively. Spontaneous Raman scattering measurements were performed in a back-scattering configuration and by using a Jobin-Yvon T64000 spectrometer coupled with an Olympus metallographic microscope. The excitation beam was provided by the green light of an Ar^+ laser emitting at $\lambda = 514.5$ nm with a power of about 3.9 mW. The same polarization of the Raman radiation was always assured on the first window of the monochromators by using a half-wave plate after the analyser. Then we can compare the different intensities among the different polarization configurations of the recorded spectra.

We investigated spontaneous Raman polarized spectra for different scattering configurations at room temperature, in order to involve phonons propagating along different directions in RTP:Nb and in RTP for comparison. To classify the different observed vibrations, we have to take into account that the Raman active irreducible representations of the vibrational optic phonon modes in the $mm2$ orthorhombic group must include A_1, A_2, B_1 and B_2 symmetry representations [23]. Figure 4 shows the recorded spectra belonging to the $x(yy)\bar{x}$, $x(yz)\bar{x}$ and $x(zz)\bar{x}$ scattering configurations, corresponding to the A_1, B_2 and A_1 symmetry representations, respectively. These spectra involve phonons propagating along the [100] direction. Figure 5 shows the polarized spectra belonging to the $z(xx)\bar{z}$, $z(xy)\bar{z}$ and $z(yy)\bar{z}$ scattering configurations and corresponding to A_1, A_2 and A_1 symmetry representations respectively. They involve phonons propagating along the [001] direction. Phonons propagating along the [010] direction have not been shown for the sake of brevity and because of the similarities observed with phonons propagating along the [100] direction. Tables 3 and 4 give the positions of the principal modes of vibration marked out in wavenumbers, as well as a classification of the strength of their intensity and their assignment for this configuration in RTP and RTP:Nb for comparison.

The recorded Raman spectra have revealed a complicated structure with about 100 peaks of very different intensities for both RTP and RTP:Nb samples due to the complexity of their crystallographic structure. Moreover, we observed a general broadening of the lines in RTP:Nb compared to RTP, which was previously observed in other compounds and assigned to an inhomogeneous structure [24]. By comparing the Raman spectra of RTP and RTP:Nb crystals given in figures 4, and 5, and from the analysis of the position of the principal modes of vibrations given in tables 3 and 4, we can distinguish between modes involving mostly the TiO_6 group or the PO_4 or Rb^+ groups. Indeed, as we reported in the previous sections, Nb substitutes Ti in the structure, and modes corresponding to the TiO_6 group are the only ones affected by this substitution. The most intense structures in all the spectra, located around 203, 265 and 693 cm^{-1}, arise from vibrations involving the TiO_6 octahedra. The ν_1 mode, a symmetric Ti–O stretching vibration [23], is the most intense peak in the region of the high-frequency modes, located at around 693 cm^{-1}. The high intensity associated with this band in RTP

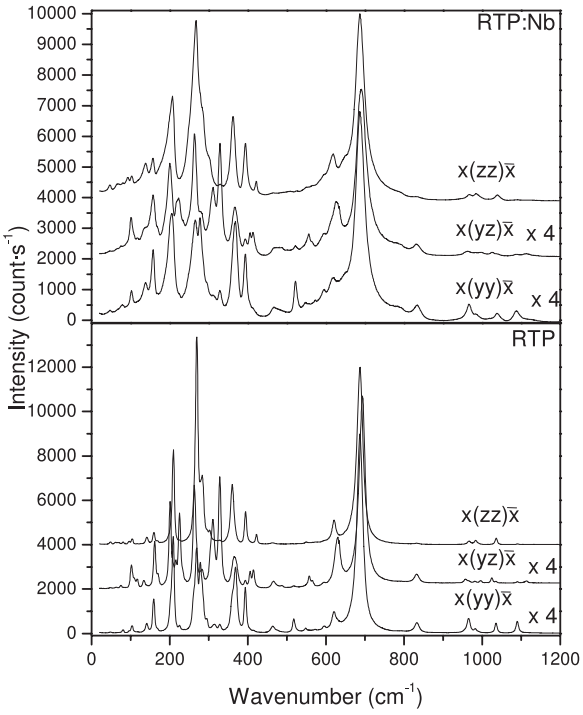

Figure 4. Raman spectra recorded at room temperature for RTP and in RTP:Nb as a function of the wavenumber in the back-scattering geometry for the $x(yy)\bar{x}$, $x(yz)\bar{x}$ and $x(zz)\bar{x}$ configurations. The $x(yy)\bar{x}$ and the $x(yz)\bar{x}$ configurations have been enhanced fourfold for a better comparison with the $x(zz)\bar{x}$ configuration.

reveals a highly ordered structure. As the intensity is maintained for RTP:Nb crystals, the non-homogeneity observed by the broadening of the bands does not affect the order of the structure, as observed in other analogues to KTP [25]. Peaks with the highest intensities, appearing around 280 and 700 cm^{-1}, have been reported in KTP, making it an excellent candidate for stimulated Raman converters or oscillators [23]. Therefore, we expect that such peaks observed in RTP and RTP:Nb from figures 4 and 5 lead to the same properties in these samples. The ν_2 mode, which is a pure bond stretching vibration, occurs at a lower energy and appears between 616 and 633 cm^{-1}, depending on the polarization. The ν_4 mode, considered as a combination of stretching and bending vibrations, appears with peaks between 311 and 330 cm^{-1} depending on the polarization scheme. The ν_5 Raman mode, an interbond angle bending vibration, is located at around 265 cm^{-1} in all the spectra. Finally, the line observed in all the spectra near 205 cm^{-1} belongs to the ν_6 mode, the other bond angle bending vibration of the structure. This mode is silent in a perfect TiO_6 octahedron [23]. In our case, however, it is activated by the distortion of the TiO_6 group in the structure. The fact that we have two crystallographically different positions for Ti in the structure [8] means that the two different TiO_6 octahedra have different Ti–O bond distances. This may be responsible for the multiple lines observed for the different vibrational modes [26]. The general shift to shorter wavenumbers in RTP:Nb, when compared to RTP, proves that Ti is substituted by a heavier ion, which is the case for Nb.

When phonons propagated along the [100] direction (see figure 4), a band was observed as a shoulder at 788 cm^{-1} for RTP:Nb crystals which has been assigned to the vibration of the Nb–O–Ti group [27]. The absence of a band corresponding to NbO_4 groups, normally located

Table 3. Position of the principal modes of vibration (cm^{-1}) recorded on the polarized spontaneous Raman scattering spectra for RTP and RTP:Nb crystals at room temperature in the $x(yy)\bar{x}$, $x(yz)\bar{x}$ and $x(zz)\bar{x}$ configurations. The intensity of the bands is expressed as vs (very small), s (small), medium (m), strong (st) and very strong (vst). When the band could not be resolved, it is indicated as sh (shoulder).

$RbTiOPO_4$			$Rb_{0.955}Ti_{0.955}Nb_{0.045}OPO_4$			
$x(yy)\bar{x}$	$x(yz)\bar{x}$	$x(zz)\bar{x}$	$x(yy)\bar{x}$	$x(yz)\bar{x}$	$x(zz)\bar{x}$	Assignation
81 vs		81 vs			81 vs	Polar vibrations Rb–O
105 s		105 vs			105 vs	
			138 s	138 sh	138 s	Translational modes Rb
143 s		143 s				
			158 m	158 m	158 m	Displacement of octahedra
160 m	160 m	160 m				
	202 st			202 st		ν_6 TiO_6
			205 st		205 st	
211 st		211 st				
	215 s					
				224 m		
228 s	228 m	228 sh				
	265 st		265 st	265 st	265 vst	ν_5 TiO_6
311 s	311 m		311 vs	311 m		ν_4 TiO_6
329 s	329 st	329 s	329 s	329 st	329 vs	
		362 st			362 st	Octahedra sharing corners
			368 st	368 m		
370 st	370 m					
395 m	395 s	395 st	395 m	395 s	395 st	ν_2 PO_4
		423 s			423 s	
465 s	465 s	465 s	465 s	465 s	465 s	ν_4 PO_4
519 m	519 vs					
			523 m	523 vs		
549 s	549 vs		549 s		549 vs	
				556 s		
	558 s					
	567 s					
574 vs			574 vs			
			618 m		618 m	ν_2 TiO_6
621 s	598 s	621 m				
				627 m		
	631 m					
688 vst		688 vst	688 vst		688 vst	ν_1 and ν_3 TiO_6
				691 vst		
	694 vst					Nb–O–Ti vibration
			788 sh	788 sh	788 sh	ν_1 PO_4
833 s	833 s	833 s	833 s	833 s	833 s	ν_3 PO_4
	997 vs			997 vs		
	1025 s			1025 vs		
1037 s		1037 s				
			1040 m		1040 s	
1091 s	1091 m		1091 m	1091 vs		
	1114 vs			1114 vs		

at 815 cm^{-1} [28], reinforces the fact that Nb ions only substitute Ti in the structure. The fully symmetric ν_1 vibration of PO_4 [26] is observed at around 833 cm^{-1} in all configurations.

Table 4. Position of the principal modes of vibration (cm^{-1}) recorded on the polarized spontaneous Raman scattering spectra for RTP and RTP:Nb crystals at room temperature in the $z\,(xx)\,\bar{z}$, $z\,(xy)\,\bar{z}$ and $z\,(yy)\,\bar{z}$ configurations. The intensity of the bands is expressed as vs (very small), s (small), medium (m) and strong (st). When the band could not be resolved, it is indicated as sh (shoulder).

$RbTiOPO_4$			$Rb_{0.955}Ti_{0.955}Nb_{0.045}OPO_4$			
$z(xx)\bar{z}$	$z(xy)\bar{z}$	$z(yy)\bar{z}$	$z(xx)\bar{z}$	$z(xy)\bar{z}$	$z(yy)\bar{z}$	Assignation
80 st	80 s		80 m			Polar vibrations Rb–O
104 st	104 st	104 m	104 st	104 st	104 m	
142 m		142 m	142 m		142 s	Translational modes Rb^+
161 s	161 m	161 st	161 s	161 m	161 st	Displacement of the octahedra
203 sh		203 sh			203 sh	ν_6 TiO_6
211 m	211 s	211 st	211 m	211 s	211 st	
	224 vs	224 s				
262 s		262 m	262 s		262 m	ν_5 TiO_6
	265 s				265 st	
313 m	313 m	313 st	313 m	313 m	313 st	ν_4 TiO_6
		330 m			330 m	
367 m	367 s	367 st	367 m	367 m	367 vst	Octahedra sharing corners
393 m	393 s	393 st	393 m	393 s	393 st	ν_2 PO_4
417 st	417 s	417 s				
			419 s	419 s		
476 st	476 vs	476 sh				ν_4 PO_4
			480 st	480 s	480 sh	
490 m	490 s	490 st			490 st	
518 st	518 s	518 st				
			523 st	523 m	523 st	
549 st	549 s	549 st	549 st	549 s	549 st	
		573 s			573 m	
627 m	627 vs	627 m	627 m	627 s	627 m	ν_2 TiO_6
	693 s	693 m		693 m	693 st	ν_1 PO_4
833 m	833 vs	833 st	833 m	833 vs	833 st	
	994 s					
				996 s		ν_3 PO_4
1006 m		1006 m				
			1011 m		1011 m	
					1023 s	
	1080 vs	1080 st		1080 s	1080 st	
1115 s		1115 m				
			1117 s		1117 m	

The ν_2 mode appears centred at around 394 cm^{-1} or at around 420 cm^{-1} according to the configuration, due to the two different structural positions of P in the framework. The ν_3 triply degenerate modes are located between 1000 and 1100 cm^{-1} and the ν_4 ones between 450 and 575 cm^{-1}. All these vibrations do not normally shift when Nb is incorporated into the crystal.

If we compare our study to the previous studies of Kugel *et al* [23], it seems reasonable to complete the internal mode picture with an analysis involving collective and coupled mode propagation in the crystal lattice. The structures lying between 138 and 188 cm^{-1} consist of a vibration in which the whole octahedron is displaced relative to the lattice. These bands tended to shift to shorter wavenumbers when Nb was present in the crystals when phonons propagated along [100] and [010] directions. Other bands involving polar vibrations between Rb^+ and the neighbouring oxygen ions are seen at around 80 and 104 cm^{-1}. Finally, the translational modes associated with Rb^+ are seen at around 140 cm^{-1}. Although a certain shifting of these bands

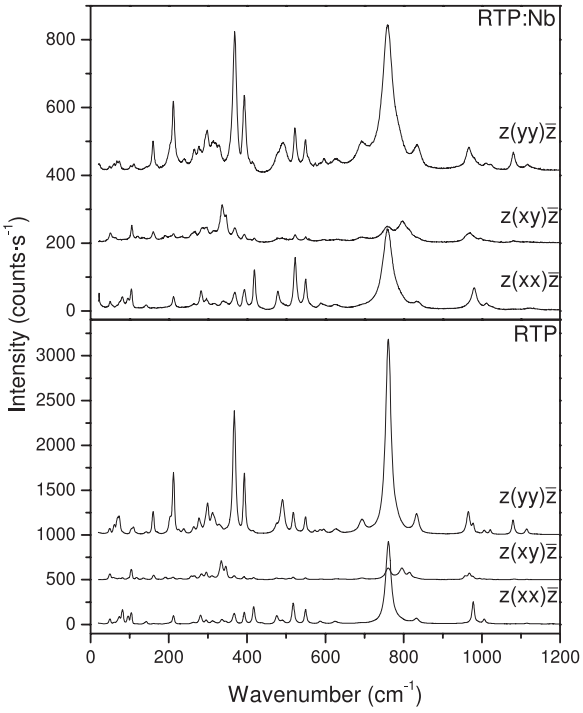

Figure 5. Raman spectra recorded at room temperature for RTP and in RTP:Nb as a function of the wavenumber in the back-scattering geometry for the $z(xx)\bar{z}$, $z(xy)\bar{z}$ and $z(yy)\bar{z}$ configurations.

to shorter wavenumbers is observed in some of the configurations, we think that this effect is more related to the presence of Rb^{+} vacancies in the RTP:Nb structure [8] than to a possible substitution of Rb^{+} by Nb^{5+}. The low frequency of the external lattice modes, involving Rb^{+} below 200 cm^{-1}, shows the weakness of the bonds between Rb and the neighbouring ions, which are essentially ionic, as reported in the literature for tungstate and molybdate crystals [26].

6. Nonlinear optical properties for frequency conversion

We have shown that RTP:Nb and RTP crystallize in the orthorhombic crystal system with the space group of symmetry $Pna2_1$. As already said, the axes of the crystallographic frame $\boldsymbol{a}$, $\boldsymbol{b}$ and $\boldsymbol{c}$ correspond to the axes of the dielectric frame x, y and z, respectively. The knowledge of the dispersion equations of the magnitudes of the three principal refractive indices, i.e. $n_x(\lambda)$, $n_y(\lambda)$ and $n_z(\lambda)$, in the whole transparency range of a crystal is of prime importance for the complete study of its non-linear optical properties. Indeed, the phase-matching directions for sum- or difference-frequency conversion depend on the ratios between the three principal refractive indices, $\frac{n_x}{n_y}(\lambda)$, $\frac{n_y}{n_z}(\lambda)$ and $\frac{n_x}{n_z}(\lambda)$ [29]. We implemented the minimum-deviation technique on prisms generally used for the determination of the dispersion equations of the three principal refractive indices. For the study of a new material, this method uses two oriented prisms and has been combined in the present study with polarized light sources emitting only in the visible and near infrared. We cut two oriented prisms of RTP:Nb and RTP with their medians parallel to the x axis and to the y axis in the x–z and y–z principal planes, respectively.

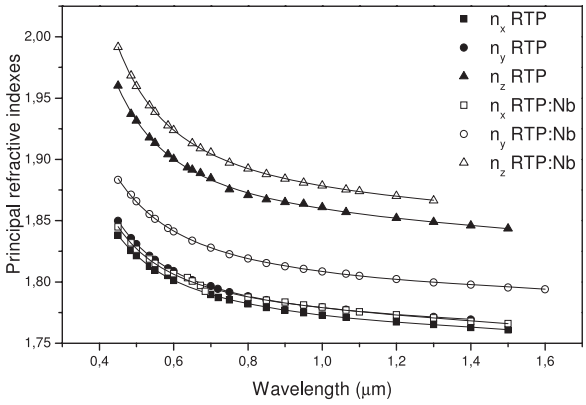

Figure 6. The three principal refractive indices as a function of the wavelength measured at room temperature in the visible and the IR regions for RTP (full figures) and RTP:Nb (open figures). The solid lines refer to the fit of all the recorded data simultaneously which is reported in this study.

Then the study of the different refractive indices relies only on a change of the polarization parallel to the x, y and z axes, successively by keeping the beam in normal incidence on the median of each of the two prisms. The three principal refractive indices n_x, n_y and n_z were measured at room temperature to an accuracy of 5×10^{-4} and as a function of the wavelength in the 0.4–1.5 μm range, by using a narrow linewidth BMI VEGA optical parametric oscillator pumped by a BMI SAGA Nd:YAG laser. The recorded data are given in figure 6 for RTP:Nb and RTP. It shows significant changes in the refractive index values between RTP:Nb and RTP: n_x is almost independent of the doping with Nb^{5+} ions, n_y and n_z significantly increase in RTP:Nb compared to RTP. Such results have been also reported in KTP:Nb compared to KTP [30]. Moreover, our data are in agreement with the literature for RTP [31, 32]. Then the $(n_z - n_x)$ birefringence is enhanced in RTP:Nb when compared to RTP. Such an increase in birefringence has been attributed to the change in the position of the UV band edge to longer wavelengths when Nb is present in KTP crystals [30]. We assume that it is the same between RTP:Nb and RTP since we reported in section 4 the same behaviour of their UV band edge. The increase of the birefringence in RTP:Nb with respect to RTP makes possible the use of these crystals for frequency doubling of light at wavelengths shorter than the one that can be doubled by RTP. This hypothesis will be confirmed later on in this paper by measuring the type II angular non-critical phase-matching (NCPM) fundamental wavelength for SHG. Note that the $(n_z - n_y)$ birefringence is smaller in RTP:Nb when compared to RTP, in opposition with what happens between KTP:Nb and KTP. This is unexpected, so we assume that it may be related to the accuracy of the measurements.

The best fit of all the recorded data simultaneously leads to the determination of three dispersion equations reliable in the scanned transparency domain only of the studied crystal. They can be used to calculate the phase-matching angles of any wavelength of this domain which are generated by sum- and difference-frequency generation. For RTP:Nb and RTP, the recorded data were simultaneous fitted with the following form of the Sellmeier equation, including one UV pole and one IR correction term:

$$n_i^2 = A_i + \frac{B_i \lambda^2}{\lambda^2 - C_i} - D_i \lambda^2 \tag{1}$$

where i stands for x, y or z and λ is in microns. We got from the fit a set of four parameters, A_i, B_i, C_i and D_i, which are listed in table 5 for RTP:Nb and RTP respectively.

Table 5. Room-temperature Sellmeier and thermo-optic coefficients of RTP and RTP:Nb.

Principal refractive index	A_i	B_i	C_i (μm^2)	D_i (μm^{-2})	$\partial n/\partial T$ (K^{-1})
			RTP		
n_x	1.6795	1.4281	0.0325	0.0119	5.6×10^{-5}
n_y	2.0360	1.0883	0.0437	0.0090	9.1×10^{-5}
n_z	2.2864	1.1280	0.0562	0.0188	6.6×10^{-5}
			RTP:Nb		
n_x	2.4753	0.6664	0.0578	0.0180	4.7×10^{-5}
n_y	1.1320	2.0885	0.0278	0.0096	7.7×10^{-5}
n_z	2.2619	1.2069	0.0594	0.0168	9.2×10^{-5}

We also studied the change of the three principal refractive indices as a function of the temperature within the 293–473 K range in both crystals. We used a microfurnace with temperature control, heating the samples homogeneously, and an He–Ne laser emitting at $\lambda = 0.6328$ μm. Then we could deduce the values of the thermo-optic coefficients that are given in table 5. As we can see, they are of the same order of magnitude for RTP and RTP:Nb. Moreover, they are similar to those of KTP [29]. The thermo-optic coefficients are almost isotropic for both crystals, which means that the birefringence of the crystals does not change with the temperature.

Finally, the type II angular non-critical phase-matching (NCPM) fundamental wavelength for SHG was measured along the principal axes. The laser source was a tunable OPO (Continuum Panther) pumped by an Nd:YAG laser (Continuum SLI-10) emitting 4 ns long (FWHM) pulses between 410 nm and 2.55 μm at a repetition rate of 10 Hz. The wavelength of the OPO was controlled by a Chromex 250 SM scanning monochromator. The laser beam was focused in normal incidence on RTP and RTP:Nb crystals cut as slabs with two faces oriented perpendicularly to the x and y axes of the dielectric frame. An achromatic half-wave plate was used to adjust the polarization of the incident beam to ensure type II NCPM SHG. We measured the corresponding fundamental wavelength λ_{NCPM}, that verifies the following relation:

$$n_\alpha\left(\frac{\lambda_{\mathrm{NCPM}}}{2}\right) = \frac{n_\alpha\left(\lambda_{\mathrm{NCPM}}\right) + n_z\left(\lambda_{\mathrm{NCPM}}\right)}{2} \tag{2}$$

where $n_\alpha = n_y$ for a propagation along the x axis, and $n_\alpha = n_x$ for a propagation along the y axis. The experimental values of λ_{NCPM} given in table 6 decrease when Nb is present in the crystals, getting closer to that of KTP, i.e. 1079.1 and 994 nm in x and y directions, respectively [33]. For RTP, our measurements were compared with success with calculated values deduced from relation [2] by using previously published equations [31, 32]. The agreement between our measurements and calculated values deduced from relation [2] by using relation [1] and table 5 is not so good. This is due to the few data available around 1.1 μm for the refractive index measurements shown in figure 6. As a consequence, such a disagreement remains for RTP:Nb. All these data are shown in table 6. We also measured the SHG conversion efficiency of RTP:Nb and RTP along these two directions and found the same order of magnitude as that of RTP. Since these two samples crystallize in the same orthorhombic system with the same group space, we suggest that the magnitudes of the non-zero elements of their second-order electric susceptibility tensor should be close.

Table 6. Fundamental wavelengths of type II angular non-critical phase-matching for SHG in RTP and RTP:Nb. They were measured and calculated along the x and y axes respectively.

	Measurements (this work)	Calculations (this work)	Calculations (reference [32])	Calculations (reference [31])
		x axis		
RTP	1144 ± 0.5	1125.1 ± 0.1	1145.8 ± 0.1	1148.6 ± 0.1
RTP:Nb	1101 ± 0.5	1319.5 ± 0.1	No equations	No equations
		y axis		
RTP	1030 ± 0.5	1053.8 ± 0.1	1033.3 ± 0.1	1029 ± 0.1
RTP:Nb	984 ± 0.5	983.6 ± 0.1	No equations	No equations

7. Conclusions

Transparent, crack- and inclusion-free isometric $Rb_{0.955}Ti_{0.955}Nb_{0.045}OPO_4$ crystals have been grown using the TSSG method and crystal seeds with millimetric dimensions. The structure of the crystals labelled as RTP:Nb was refined, which was confirmed by transmission spectra. Moreover, the edge in the UV region is shifted to longer wavelengths in RTP:Nb when compared to RTP. This suggests that Nb substitutes Ti positions in the structure. This is confirmed by the fact that the IR and polarized Raman bands corresponding to the PO_4 tetrahedra are not shifted when Nb is present in the crystals, while bands involving vibrations of the TiO_6 octahedra are shifted when Nb is present in the crystals. Finally, the chromatic dispersion curves were measured and used to calculate the fundamental wavelengths corresponding to the type II angular non-critical phase-matching for second-harmonic generation (SHG), λ_{NCPM}. They were compared with success to measured values of λ_{NCPM}, which decrease in RTP:Nb when compared to RTP, approaching that of KTP. The associated conversion efficiencies remain of the order of that of RTP, leading to RTP:Nb as a new very good non-linear crystal.

Acknowledgments

This work was supported by CICyT of the Spanish Government under MAT-2005-06354-C03-02, MAT-2004-20471-E and CIT-020400-2005-14, and by CIRIT of the Catalonian Government under 2005SGR658.

References

[1] Bierlein J D and Vanherzeele H 1989 *J. Opt. Soc. Am.* B **6** 622–33
[2] Chung J and Siegman A E 1993 *J. Opt. Soc. Am.* B **10** 2201–10
[3] Masse R and Grenier J C 1971 *Bull. Soc. Fr. Minéral. Cristallogr.* **94** 437–9
[4] Oseledchik Y S, Pisarevsky A I, Proscirnin A L, Starshenko V V and Svitanko N V 1994 *Opt. Mater.* **3** 237–42
[5] Karlsson H, Laurell F and Cheng L K 1999 *Appl. Phys. Lett.* **74** 1519–21
[6] Zaldo C, Rico M, Díaz F and Carvajal J J 1999 *Opt. Mater.* **13** 175–80
[7] Carvajal J J, Solé R, Gavaldà J, Massons J, Aguiló M and Díaz F 2003 *Opt. Mater.* **24** 425–30
[8] Carvajal J J, García-Muñoz J L, Solé R, Gavaldà J, Massons J, Solans X, Díaz F and Aguiló M 2003 *Chem. Mater.* **15** 2338–45
[9] Carvajal J J, Nikolov V, Solé R, Gavaldà J, Massons J, Rico M, Zaldo C, Aguiló M and Díaz F 2000 *Chem. Mater.* **12** 3171–80
[10] Carvajal J J, Woensdregt C F, Solé R, Díaz F and Aguiló M 2006 *Cryst. Growth Des.* **6** 2667–73

[11] Sheldrick G M 1997 *SHELXS97. A Computer Program for Crystal Structure Determination* University of Göttingen, Germany
[12] Thomas P A, Mayo S C and Watts B E 1992 *Acta Crystallogr.* B **48** 401–7
[13] Carvajal J J, Solé R, Gavaldà J, Massons J, Díaz F and Aguiló M 2003 *Chem. Mater.* **15** 2730–6
[14] Zumsteg F C, Bierlein J D and Gier T E 1976 *J. Appl. Phys.* **47** 4980–5
[15] Thomas P A and Watts B E 1990 *Solid State Commun.* **73** 97–100
[16] Losevskaya T Y, Alekseeva O A, Yanovskii V K, Voronkova V I, Sorokina N I, Simonov V I, Stefanovich S Y, Ivanov S A, Eriksson S and Zverkov S A 2000 *Crystallogr. Rep.* **45** 739–43
[17] Jacco J C and Loiacono G M 1991 *Appl. Phys. Lett.* **58** 560–2
[18] Hansson G, Karlsson H, Wang S and Laurell F 2000 *Appl. Opt.* **39** 5058–69
[19] Martín M J, Bravo D, Solé R, Díaz F, López F J and Zaldo C 1994 *J. Appl. Phys.* **76** 7510–8
[20] Zysset B, Biaggio I and Gunter P 1992 *J. Opt. Soc. Am.* B **9** 380–6
[21] Herzberg G 1975 *Infrared and Raman Spectra of Polyatomic Molecules* (New York: Van Nostrand)
[22] Jacco J C 1986 *Mater. Res. Bull.* **21** 1189–94
[23] Kugel G E, Bréhat F, Wyncke B, Fontana M D, Marnier G, Carabatos-Nedelec C and Mangin J 1988 *J. Phys. C: Solid State Phys.* **21** 5565–84
[24] Voronko V K, Sobol A A, Ushakov S N and Tsybal L I 2000 *Inorg. Mater.* **36** 947–53
[25] Bushiri M J and Nayar V U 2001 *J. Non Linear Opt. Phys. Mater.* **10** 345–54
[26] Basiev T, Sobol A A, Voronko Y K and Zverev P G 2000 *Opt. Mater.* **15** 205–16
[27] Balachandran U and Eror N G 1982 *J. Mater. Sci. Lett.* **1** 374–6
[28] Blasse G 1973 *J. Solid State Chem.* **7** 169–71
[29] Dmitriev V G, Gurzadyan G G and Nikogosyan D N 1991 *Handbook of Nonlinear Optical Materials* (Berlin: Springer)
[30] Cheng L T, Cheng L K, Harlow R L and Bierlein J D 1994 *Appl. Phys. Lett.* **64** 155–7
[31] Oseledchik Y S, Pisarevsky A I, Prosvirnin A L, Lopatko V N, Kholodenkov L E, Titov F F, Demidovich A A and Shkadarevich A P 1990 *Proc. Conf. on Lasers Optics* (Leningrad: Leningrad University Press)
[32] Guillien Y, Ménaert B, Fève J P, Segonds P, Douady J, Boulanger B and Pacaud O 2003 *Opt. Mater.* **22** 155–62
[33] Boulanger B, Fève J P, Marnier G and Ménaert B 1998 *Pure Appl. Opt.* **7** 239–56